Electronic Supplementary Material (ESI) for Materials Chemistry Frontiers.

Supporting information

2D thin sheet composed of $Co_{5.47}N$-MgO embedded in carbon as a durable catalyst for the reduction of aromatic nitro-compounds

Chengxu Jin,[a] Ying Gu,[a] Zhihui Li,[a] Siyu Wang,[a] Nan Wang,[a] Yanqing Jiao,[a]* Buhe Bateer,[b] Chungui Tian[a]*

[a]*Key Laboratory of Functional Inorganic Material Chemistry, Ministry of Education of the People's Republic of China, Heilongjiang University. Harbin 150080, China*
E-mail: jiaoyq617outlook.com; tianchungui@hlju.edu.cn.
[b]*College of Materials and Chemical Engineering,*
Heilongjiang Institute of Technology, Harbin 150050, China

Table S1. The samples and the corresponding preparation conditions.

Name	Reaction Condition	2-MIM
$Co_{5.47}N$-MgO-1	(1) 25 °C ⟶ 410 °C (3 h) (2) Washing (3) 25 °C ⟶ 620 °C (4 h)	√
$Co_{5.47}N$-MgO-2	(1) 25°C ⟶ 620°C (4 h) (2) Washing	√
$Co_{5.47}N$-MgO-3	(1) 25 °C ⟶ 410 °C (3 h) (2) 410 °C ⟶ 550 °C (4 h) (3) Washing	√
$Co_{5.47}N$-MgO-4	(1) 25 °C ⟶ 410 °C (3 h) (2) 410 °C ⟶ 670 °C (4 h) (3) Washing	√
Co-MgO	(1) 25 °C ⟶ 410 °C (3 h) (2) 410 °C ⟶ 620 °C (4 h) (3) Washing	×

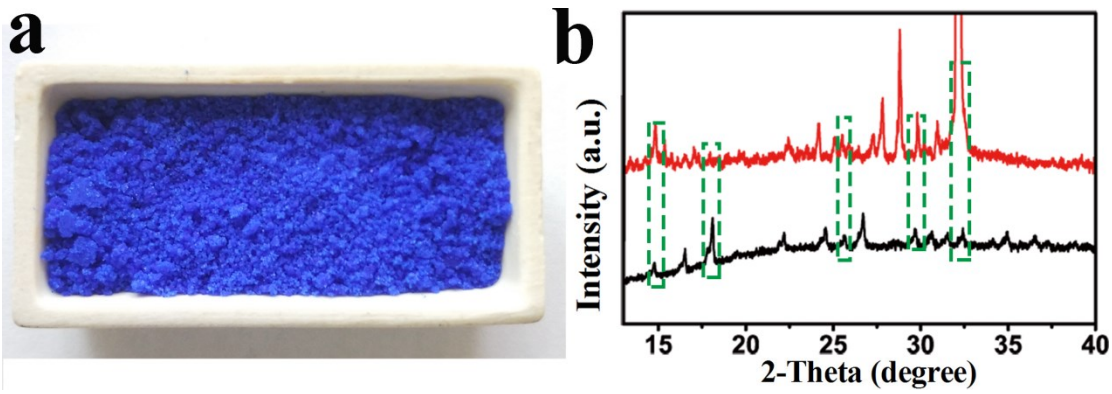

Figure S1. (a) The photograph of the product after grinding the mixture of $Co(NO_3)_2 \cdot 6H_2O$, 2-MIM and salts (NaCl, KCl and $MgCl_2$); and (b) XRD patterns of

the above sample (red line) and ZIF-67 (black line).

As shown in Figure S1a, after grinding the mixture of $Co(NO_3)_2 \cdot 6H_2O$, 2-methylimidazole and salts (NaCl, KCl and $MgCl_2$), the sample changes to blue powder, which may be due to the formation of ZIF-67-like particles in the system. To prove this, the phase composition of the sample was analyzed by X-ray diffraction (XRD). As shown in Figure S1b, the sample displays typical diffraction peaks at 14.7°, 18.0°, 25.6°, 29.6° and 32.4°, corresponding to the diffraction peaks of ZIF-67, respectively, implying there are some ZIF-67-like particles in the system during the grinding process. However, the intensity of the diffraction peak is weak, which may be caused by the low crystallinity in the grinding process.

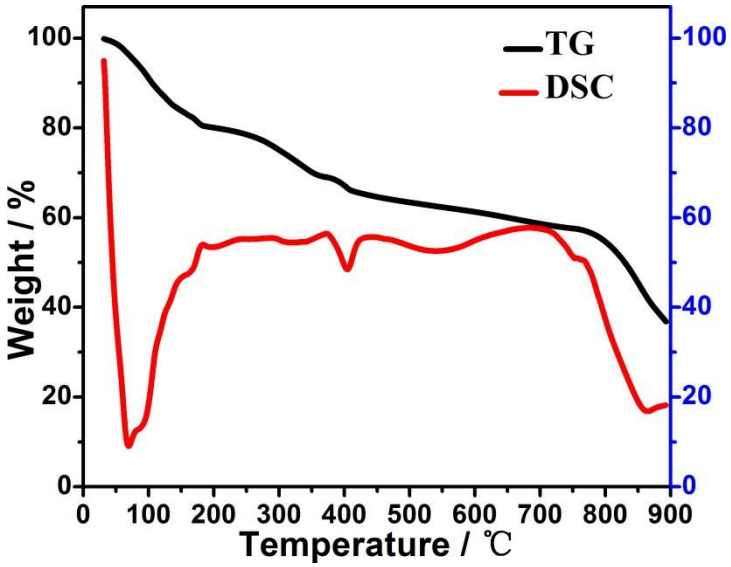

Figure S2. Thermogravimetric analysis of the product after grinding the mixture of $Co(NO_3)_2 \cdot 6H_2O$, 2-MIM and salts (NaCl, KCl and $MgCl_2$).

Thermogravimetric analysis manifests that the sample from grinding the mixture of $Co(NO_3)_2 \cdot 6H_2O$, 2-MIM and salts (NaCl, KCl and $MgCl_2$) has the melting point about 405 °C (Figure S2).

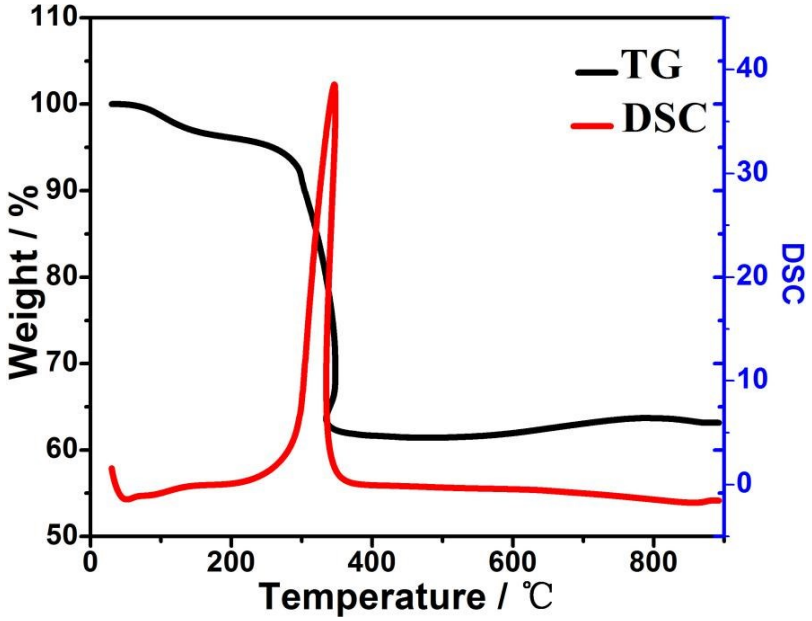

Figure S3. Thermogravimetric analysis of the 2D $Co_{5.47}N$-MgO@C.

Thermogravimetric analysis was carried out to comfirm whether there is any amorphous carbon (Fig. S3). The content of carbon component is about 34.3 wt %, which can prevent the corresponding catalyst from erosion, further boosting catalytic stability. It is noteworthy that the organic carbon layer is derived from 2-MIM, implying tight contact between $Co_{5.47}N$ and MgO.

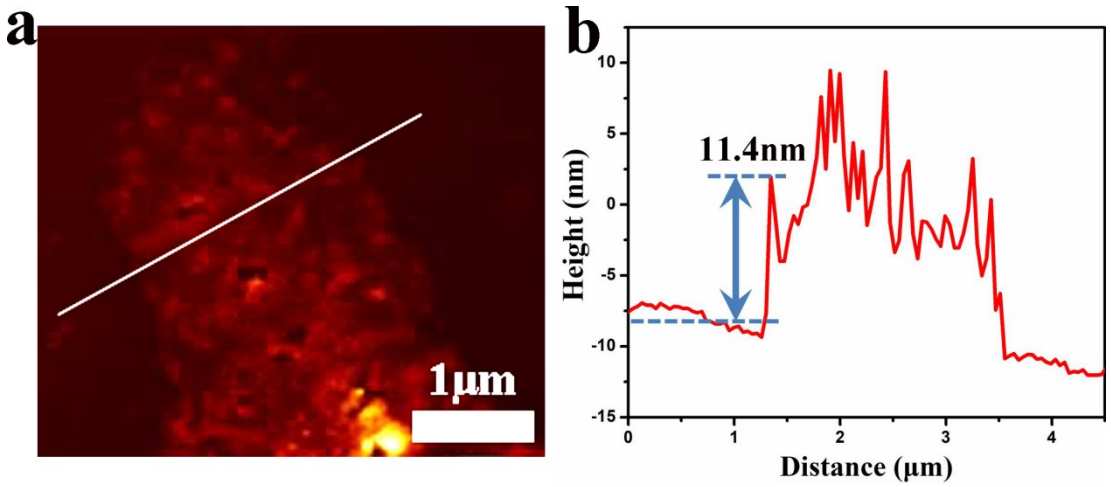

Figure S4. (a) AFM image and (b) corresponding height profiles along the white line of the 2D $Co_{5.47}N$-MgO@C.

The thickness of 2D $Co_{5.47}N$-MgO@C was characterized by atomic force microscopy (AFM). As shown in Figure S3a, 2D $Co_{5.47}N$-MgO@C has an obvious flaky structure, and its thickness is only 11.4 nm (Figure S4b). This further illustrates

the thin sheet structure of 2D $Co_{5.47}$N-MgO@C. This structure is beneficial to good catalytic performance.

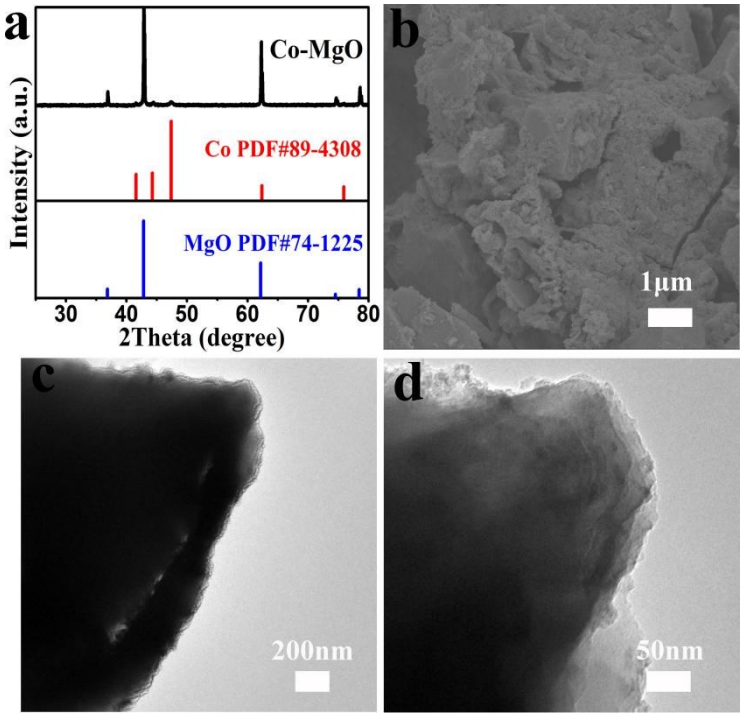

Figure S5. The XRD pattern (a), typical SEM images (b) and TEM images(c and d) of sample (Co-MgO).

XRD pattern (Fig. S5a) displays the characteristic peaks assigned to MgO and Co. The morphology of the sample Co-MgO without adding 2-MIM was studied by scanning electron microscope (SEM) and transmission electron microscope (TEM). As shown in Figure S5b, the SEM shows a massive structure of large particles. It is explained that cobalt component could not be stabilized without 2-MIM and tends to form a larger mass of particles, rather than a 2D flake structure. The TEM images also show obviously that the morphology of the synthesized sample is a massive stacked structure (Figure S5c and S5d).

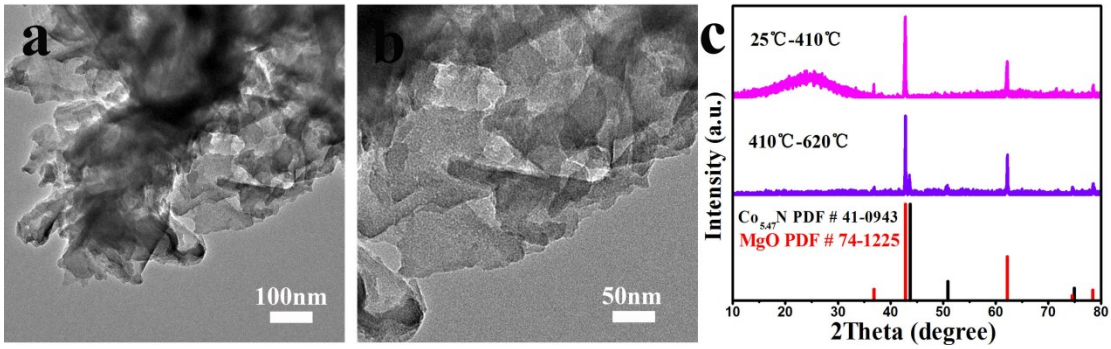

Figure S6. (a and b) Typical TEM images of the intermediate (25 °C-410 °C) during the preparation process of $Co_{5.47}N$-MgO-1; (c) XRD patterns of the intermediate after first stage heating (25 °C-410 °C) and the corresponding product after second stage heating (410 °C-620 °C).

The morphology of the intermediate (25 °C-410 °C) during the preparation process of $Co_{5.47}N$-MgO-1 was studied by TEM. As shown in Figure S6a and S6b, the TEM images reveal that the sample has obvious thin-layer structure, indicating that the sample has already started to form flake structure at 410 °C. This further indicates that the stepwise heating is beneficial to promote the formation of stabilized intermediate containing Co species. It is very important for synthesizing 2D $Co_{5.47}N$-MgO@C. In addition, the phase composition of $Co_{5.47}N$-MgO-1 sample was analyzed by X-ray diffraction (XRD). The XRD pattern of the intermediate only shows the characteristic peaks assigned to MgO, in which there are no obvious peaks belonged to $Co_{5.47}N$. (Fig. S6c). After separated from molten salts, the solid was additionally calcined in NH_3 at 620 °C for 3 h. The product composed of $Co_{5.47}N$ and MgO was finally obtained (Fig. S6c). The above results further indicate both Co and Mg species are included in the intermediate, in which the Co species are amorphous. It shows that the intermediate of the product begins to form at 410 °C. After removing the salts, the sample was again heated to 620 °C, giving rise to $Co_{5.47}N$-MgO-1. The phase composition of the obtained product was characterized by XRD, and there are obvious diffraction peaks of $Co_{5.47}N$ appeared. This further shows that the stepwise heating is very necessary for the formation of stable intermediates.

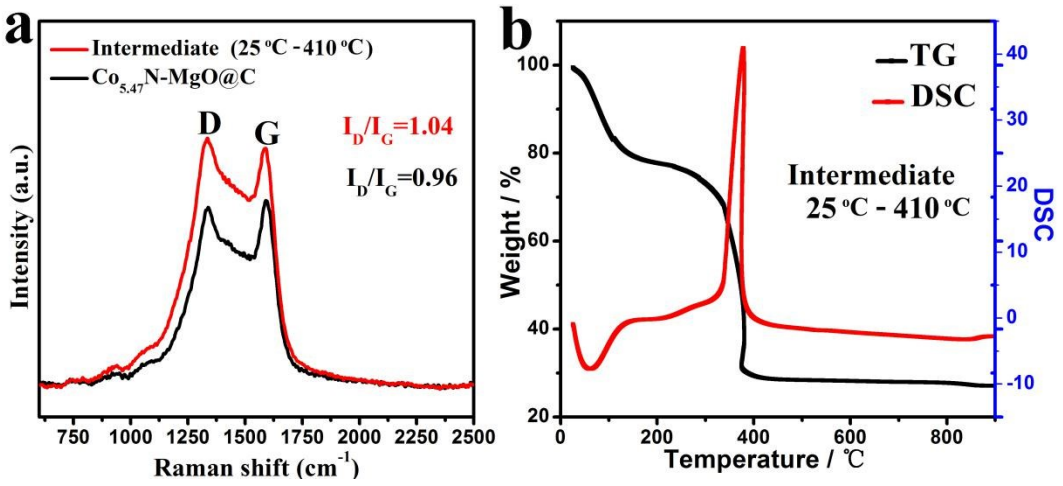

Figure S7 (a) Raman spectra of the intermediate after the first heating stage (25 °C-410 °C) and $Co_{5.47}N$-MgO@C NS; (b) Thermogravimetric analysis of the intermediate separated from the first heating stage (25 °C-410 °C) in the synthesis.

There are two prominent peaks located at around 1369 and 1590 cm^{-1}, assigned to the D and G bands, respectively (Fg S7a). The intensities of D peaks in both the intermediate after the first heating stage (25 °C-410 °C) and $Co_{5.47}N$-MgO@C NS are so strong, implying the carbon components in the above samples are amorphous. Compared with $Co_{5.47}N$-MgO@C NS, the intermediate after the first stage heating (25 °C-410 °C) presents higher intensity ratio of the D/G peak (I_D/I_G), illustrating that the carbon component in the intermediate is more disorder. Besides, thermogravimetric analysis was carried out to comfirm the content of carbon component (Fg S7b). The content of carbon component is about 48.9 wt %, far greater than that (34.3 wt %) of $Co_{5.47}N$-MgO@C NS (Fg S3). Combined with the XRD pattern, we can draw a conclusion that the amorphous Co stabilized by carbon was successfully transformed to $Co_{5.47}N$, simultaneously losing some carbon under the high temperature during the second calcination stage.

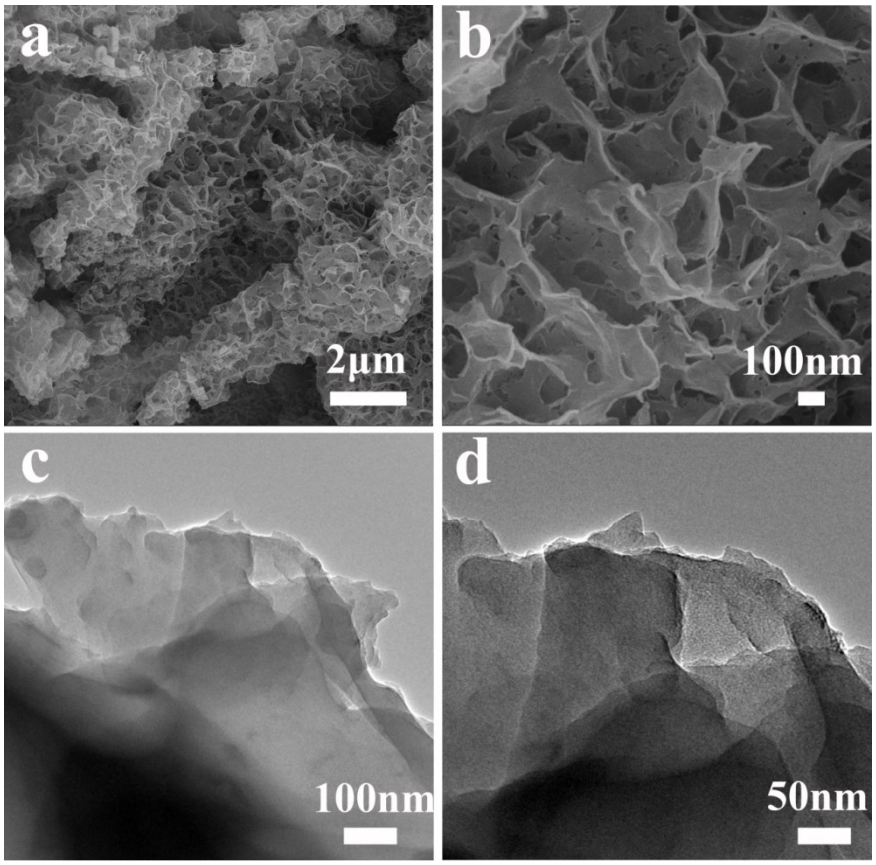

Figure S8. Typical SEM images (a and b) and TEM images(c and d) of $Co_{5.47}N$-MgO-2 (25 ^{o}C-620 ^{o}C).

The morphology of the sample by direct heating to 620 ^{o}C was studied by SEM and TEM. As shown in Figure S8a and S8b, the SEM shows that there are a large number of holes on the surface of the sample, indicating that the direct heating destroys the structure. As a result, the flaky could not be well maintained. In addition, the thin layer structure with holes on the surface can be seen obviously on the image of TEM (Figure S8c and S8d). And it may also affect the catalytic performance of the sample. This shows that when heating up directly, there is not enough time to stabilize the 2D nanosheets, leading to the rapid growth and connection of the nanosheets. This is not conducive to the synthesis of the target product. This further shows that the stage heating is very necessary for the synthesis of 2D $Co_{5.47}N$-MgO@C.

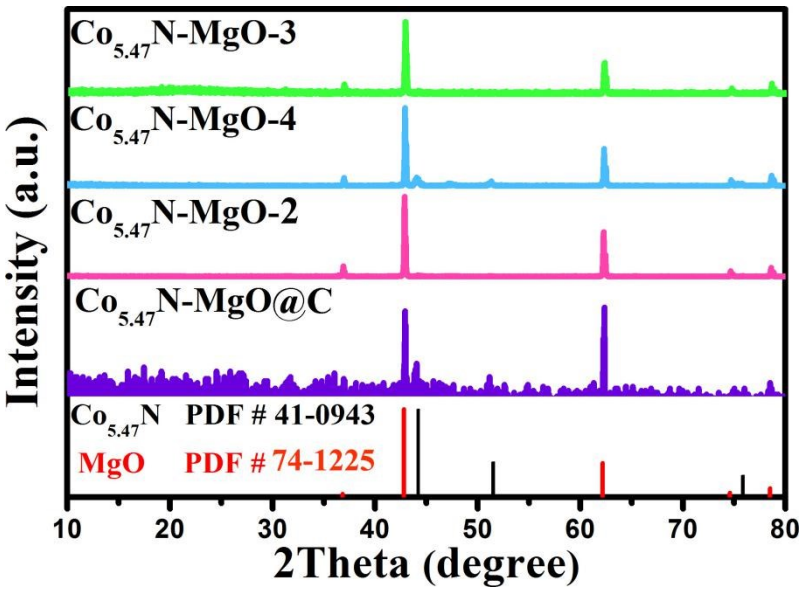

Figure S9. XRD of $Co_{5.47}N$-MgO-2, $Co_{5.47}N$-MgO-3 and $Co_{5.47}N$-MgO-4 at different temperature.

This further confirms the previous synthesis of nanosheets containing cobalt nitride. As shown in Figure S9, the XRD of $Co_{5.47}N$-MgO-2, $Co_{5.47}N$-MgO-3 and $Co_{5.47}N$-MgO-4 at different temperature. The XRD of $Co_{5.47}N$-MgO-2 shows unapparent peaks of nitrides (Fig. S9). The results emphasize that one step direct calcination is not conducive to the nitridation of Co species. The 2D nanosheets can be formed at first step (low-temperature treatment at 410 ℃). In the case of continual two-step heating process, the heating temperature of the second step is also an important factor. Two control samples were obtained under the similar condition expect the second calcination temperatures were 550 ℃ and 670 ℃, named as $Co_{5.47}N$-MgO-3 and $Co_{5.47}N$-MgO-4. When the temperature of the second-step heating is reduced to 550 ℃, the peaks of $Co_{5.47}N$ are not obvious (Fig. S9), indicating the low crystallinity of $Co_{5.47}N$ in the sample due to low reactivity of NH_3 at lower temperature. When the temperature is raised to 670 ℃, the sample shows thick sheets (Fig. S12a). The peaks of $Co_{5.47}N$ show very low, implying the low N content, due to the additional reduction of Co_xN by NH_3 to form Co metals at high temperature.

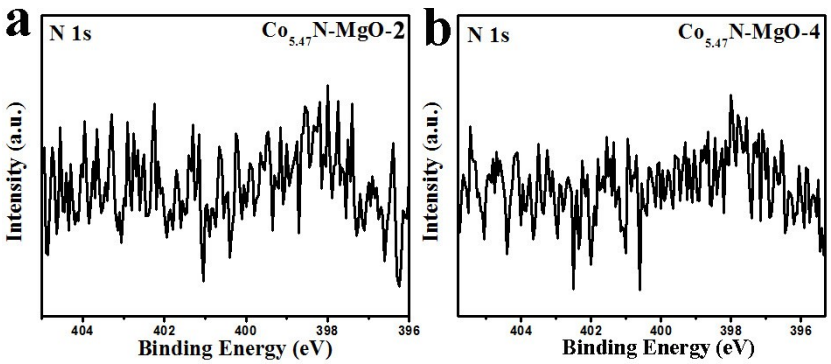

Figure S10. XPS of N 1s for (a) $Co_{5.47}N$-MgO-2 and (b) $Co_{5.47}N$-MgO-4 at different temperature.

The elemental composition and valence electrons of the samples were identified by X-ray photoelectron spectroscopy (XPS). As shown in Figure S10a, when the calcination mode was changed to direct heating, sample $Co_{5.47}N$-MgO-2 was synthesized. Compared with the sample by heated in two steps, the XPS diagram shows that the peak of N 1s is not obvious. This emphasizes that direct heating at higher temperature is not conducive to the nitridation of Co species. This further illustrates the importance of staging heat on sample synthesis. When the calcination temperature was increased to 670 ^{o}C, the N 1s XPS still shows very weak peak (Figure S10b), implying the lower N content due to the further reduction of Co_xN to Co metal by NH_3 at high temperature. To sum up, the selection of appropriate calcination temperature and calcination method is very important for the synthesis of the product.

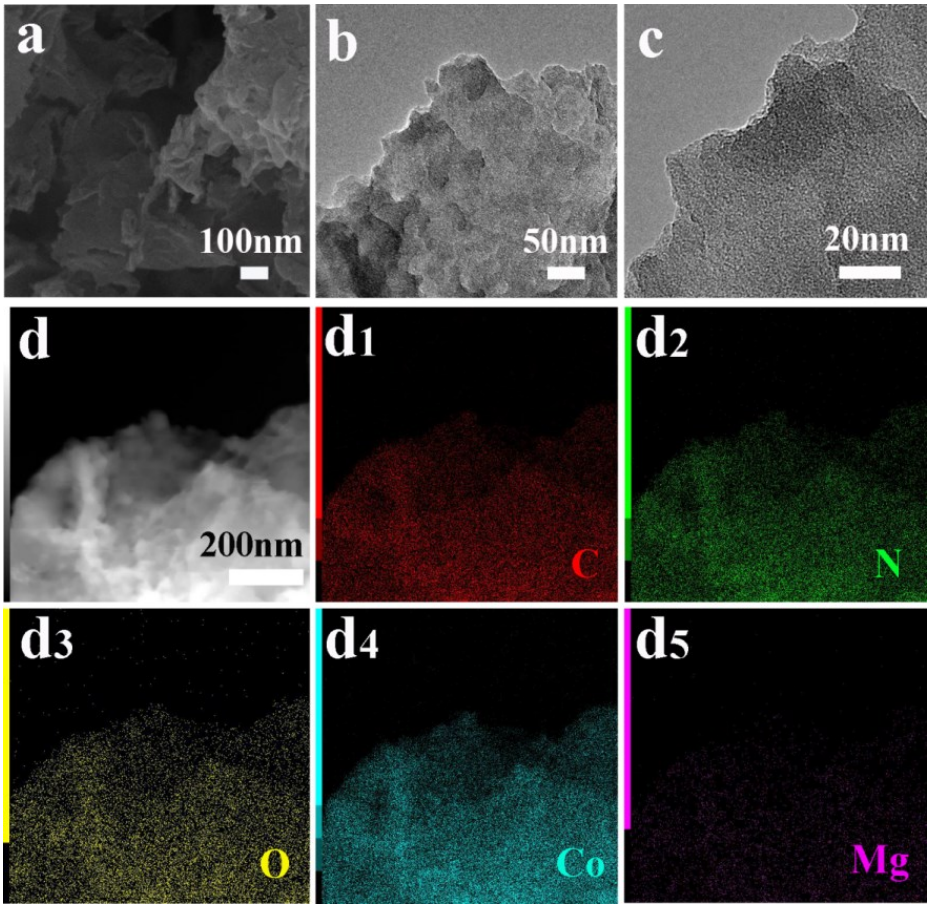

Figure S11. Typical SEM images (a) and TEM images (b and c), (d) EDS elemental mapping images of $Co_{5.47}N$-MgO-3 (410 ^{o}C-550 ^{o}C).

The morphology of the sample was studied by scanning electron microscope (SEM) and transmission electron microscope (TEM) when the calcination temperature was reduced to 550 ^{o}C. As shown in Figure S11a, the SEM shows that the sample is still flaky. The TEM image also reveals the structure of the thin layer (Figure S11b and S11c), and it is obvious that some dense and uniform particles are uniformly distributed on the sheet. In addition, we use energy dispersive X-ray energy spectrum (EDS) to detect the distribution of elements in the sample, as shown in Figure S11. EDS element mapping shows that C, N, O, Mg and Co elements are uniformly distributed in the sample.

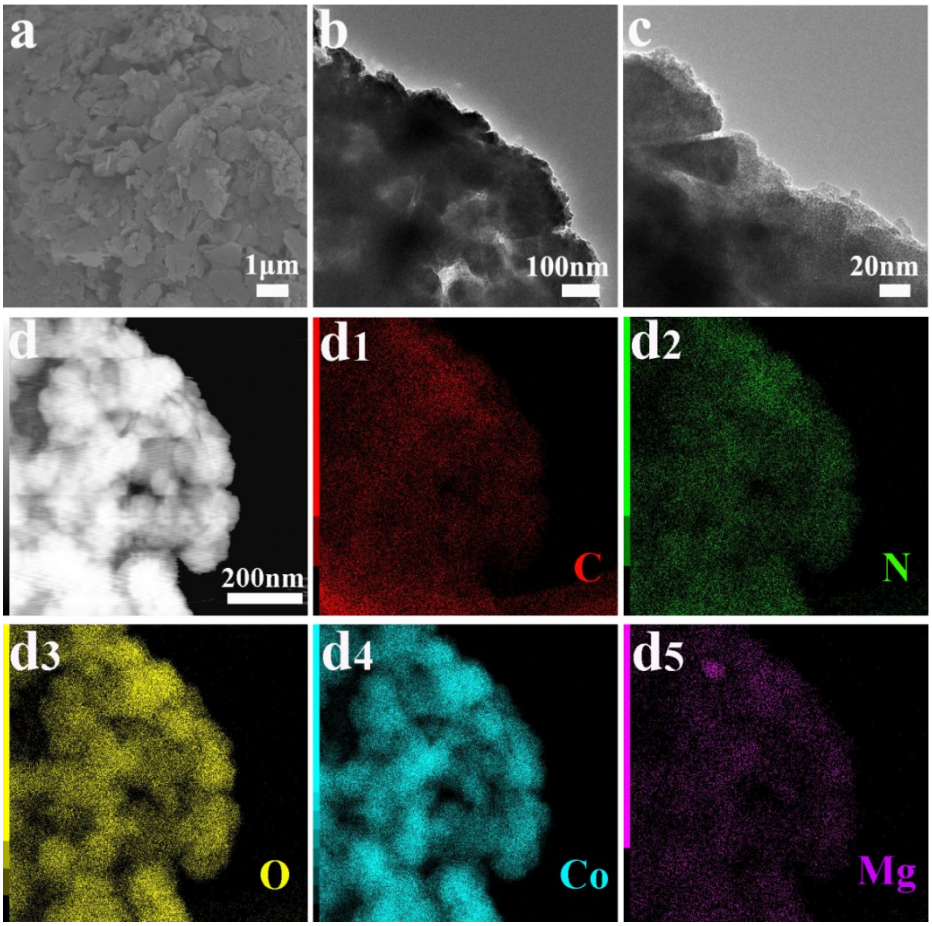

Figure S12. Typical SEM images (a) and TEM images (b and c), (d) EDS elemental mapping images of $Co_{5.47}N$-MgO-4(410 ^{o}C-670 ^{o}C).

When the calcination temperature was increased to 670 ^{o}C, the morphology of the corresponding sample was studied by SEM and TEM. As shown in Figure S12a, the SEM shows that the sample is still a flaky structure, but the sheets become thick. TEM images show that there are most of the larger particles in the sample (Figure S12b and S12c). This may be due to the excessive reduction and aggregation of particles caused by high temperature. It may affect the catalytic performance of the sample. Moreover, the distribution of elements in the sample was characterized by energy dispersive X-ray spectroscopy (EDS). As shown in Figure S12d, EDS element mapping shows that C, N, O, Mg and Co elements are uniformly distributed in the sample.

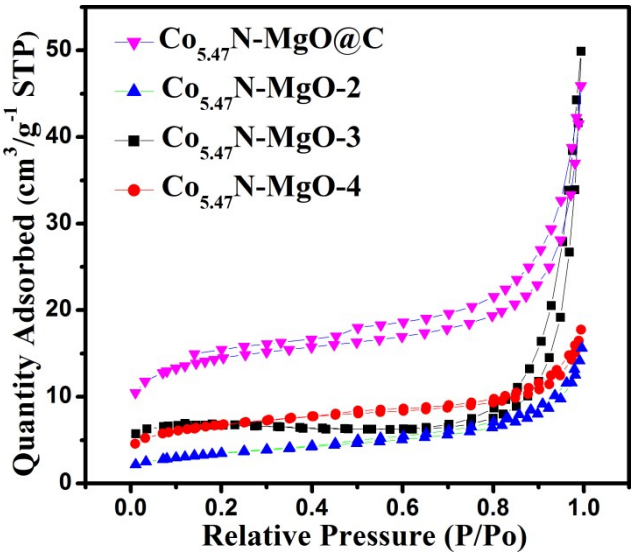

Figure S13. Adsorption-desorption isotherms for 2D $Co_{5.47}$N-MgO@C NS, $Co_{5.47}$N-MgO-2, $Co_{5.47}$N-MgO-3 and $Co_{5.47}$N-MgO-4.

N_2 adsorption-desorption measurement was carried out to analyze the surface area of the samples by BET method. As shown in Fig. S13, the specific surface areas of $Co_{5.47}$N-MgO@C NS, $Co_{5.47}$N-MgO-2, $Co_{5.47}$N-MgO-3 and $Co_{5.47}$N-MgO-4 are 50.2, 12.4, 22.9 and 23.9 m^2/g, respectively. Obviously, the 2D $Co_{5.47}$N-MgO@C NS shows the highest specific area, affording the abundant reactive catalytic surface in favor of the catalytic reaction process.

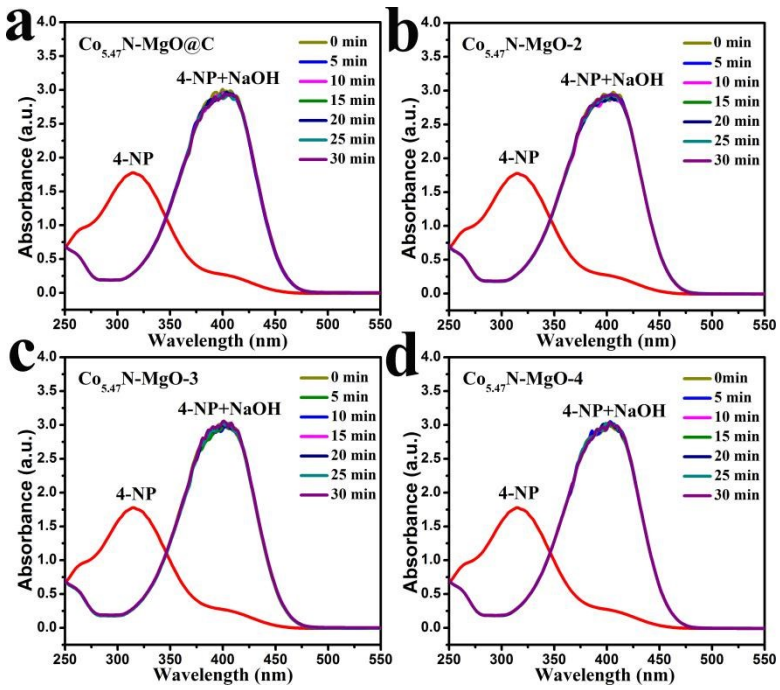

Figure S14. UV-vis absorption spectra of the deprotonated 4-NP solution (tuned pH

by NaOH) containing $Co_{5.47}N$-MgO@C NS (a), $Co_{5.47}N$-MgO-2 (b), $Co_{5.47}N$-MgO-3 (c) and $Co_{5.47}N$-MgO-4 (d).

The pH of the solution containing 4-NP and $NaBH_4$ was measured as 9.8. Hence, we adjusted pH of the 4-NP solution by adding dilute NaOH solution to reach 9.8, in order to obtain nitrophenolate ions. The pale yellow 4-NP aqueous solution turns into the bright yellow after adding NaOH, which is caused by the 4-NP deprotonation. The absorption peak located at 400 nm remains unchanged after adding 2D $Co_{5.47}N$-MgO@C NS catalyst for more than 30 min (Fig. S14). Therefore, after adding $NaBH_4$, the decrease of the absorption peak intensity is due to the conversion of 4-NP to 4-AP, rather than the adsorption function of nitrophenolate ions. The above test confirms 2D $Co_{5.47}N$-MgO@C NS indeed acts as an efficient catalyst to achieve the conversion from 4-NP to 4-AP by using $NaBH_4$ as a reducing agent.

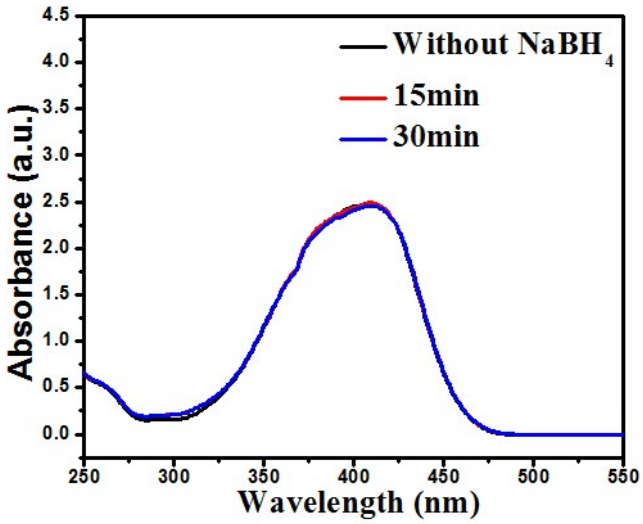

Figure S15. UV-vis absorption spectra of the 4-NP solution containing $Co_{5.47}N$-MgO@C NS.

Under the same other conditions, the Ultraviolet-visible (UV-vis) spectrum was used to analyze the change of the absorption peak when only 2D $Co_{5.47}N$-MgO@C catalyst was added without the present of $NaBH_4$. As shown in Figure S15, the absorption peak at 310 nm still shifts to 400 nm, which may be due to the deprotonation of 4-NP caused by the basicity of MgO. The experimental results show that the absorption peak at 400 min remains unchanged only when the 2D $Co_{5.47}N$-MgO@C catalyst is added for more than 30 nm. This shows that this kind of conversion is

impossible without the help of 2D $Co_{5.47}N$-MgO@C catalyst. This further illustrates its heterogeneous catalytic properties.

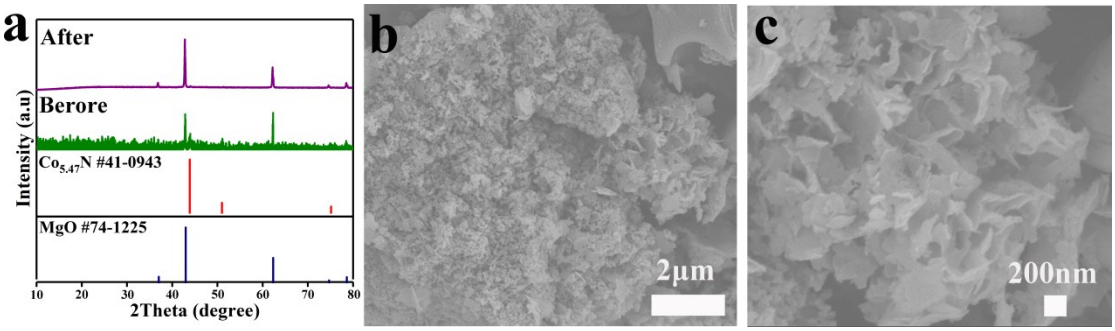

Figure S16. (a) XRD of catalyst $Co_{5.47}N$-MgO before and after 4-NP conversion to 4-AP; (b and c) SEM of catalyst $Co_{5.47}N$-MgO after 4-NP conversion to 4-AP.

The phase composition of the transformed 2D $Co_{5.47}N$-MgO@C sample was analyzed by X-ray diffraction (XRD). As shown in Figure S16a, there is almost no change in the XRD of 2D $Co_{5.47}N$-MgO@C after use, indicating that no new substance is formed in the reaction process. In addition, SEM images show an obvious 2D flake structure (Figure S16b and S16c). The morphology of the material remains basically unchanged, which indicates that 2D $Co_{5.47}N$-MgO@C has good stability. This also further explains the reason why the cyclic stability of its performance is better.

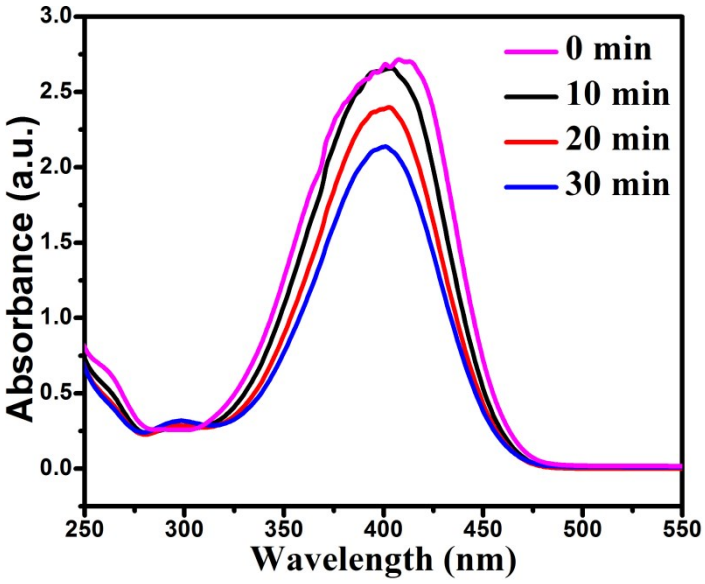

Figure S17. UV-vis absorption spectra of the 4-NP solution containing Co-MgO.

Taking the reduction of 4-NP to 4-AP as a model, the catalytic performance of the sample Co-MgO synthesized without adding 2-MIM was evaluated. As shown in Figure S17, when the sample was used as catalyst, the absorption peak of the solution at 400 nm did not change significantly after 30 min, showing poor performance. This may be due to the fact that cobalt particles could not be stabilized without 2-MIM, and tend to aggregate. Therefore, the target product could not be synthesized, resulting in the poor performance. This further illustrates the necessity of 2-MIM in the synthesis process.

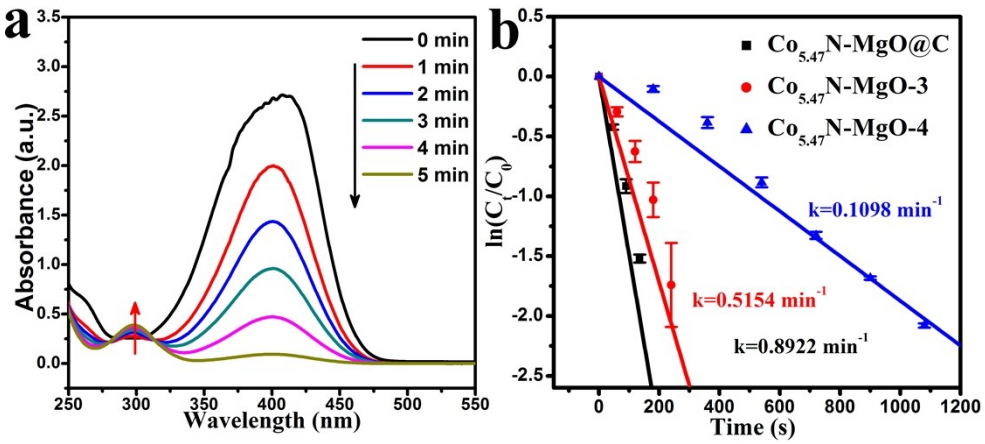

Figure S18. (a) UV-vis absorption spectra of the 4-NP solution containing $Co_{5.47}N$-MgO-3 (the calcination temperature is 410 °C-550 °C); (b) $\ln C_t/C_0$ as a function of the reaction time at the different calcination temperatures.

Using the reduction of 4-NP to 4-AP as a model, the catalytic performances of the samples synthesized at different calcination temperatures were evaluated. As shown in Figure S18a, sample $Co_{5.47}N$-MgO-3 was synthesized when the calcination temperature was reduced to 550 °C. Compared with 2D $Co_{5.47}N$-MgO@C, the conversion time of $Co_{5.47}N$-MgO-3 is 5 min. This may be due to the decreased temperature did not reach the suitable crystallization temperature of cobalt nitride. As a result, the content of cobalt nitride in $Co_{5.47}N$-MgO-3 is low, which affects its property. A plot of $\ln(C_t/C_0)$ was linearly correlated with the reduction of 4-NP. As shown in Figure S18b, the first-order apparent rate constants (k) for 2D $Co_{5.47}N$-MgO@C, $Co_{5.47}N$-MgO-3 and $Co_{5.47}N$-MgO-4 are about 0.8922 min^{-1}, 0.5154 min^{-1} and 0.1098 min^{-1}. When the

temperature is increased to 670 °C ($Co_{5.47}N$-MgO-4), the conversion performance is poor. It is speculated that the increase of temperature will generate larger particles and smaller specific surface area of $Co_{5.47}N$-MgO-4, resulting in lower activity. At the same time, the activity of $Co_{5.47}N$-MgO-3 with flake structure is much better than that of $Co_{5.47}N$-MgO-4 composed of thicker slices. This further shows that the 2D nanosheets has a good promoting effect on the performance.

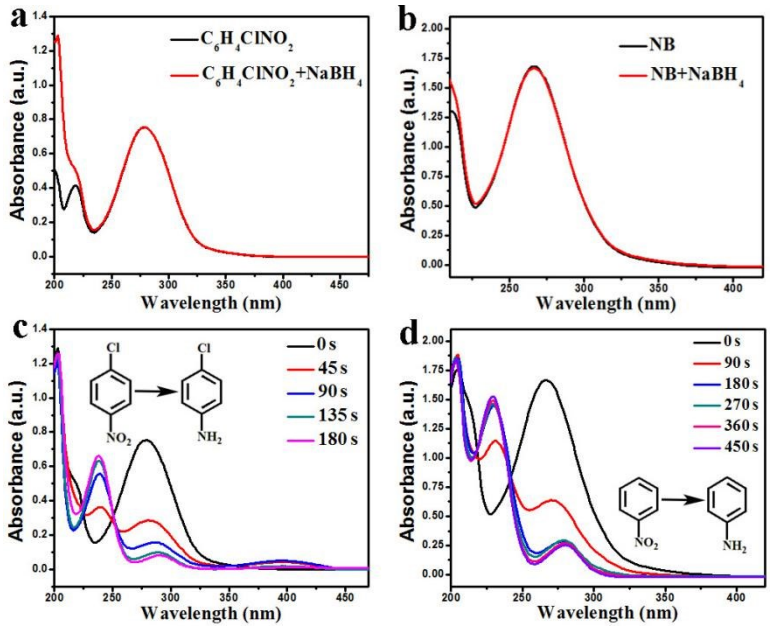

Figure S19. UV absorption before and after the addition of $NaBH_4$ into (a) $C_6H_4ClNO_2$, (b) $C_6H_5NO_2$; Change of absorbance of solution in the presence of $NaBH_4$ of (c)$C_6H_4ClNO_2$, (d) NB.

We used the catalyst to reduce $C_6H_4ClNO_2$ and $C_6H_5NO_2$ (NB). As shown in Figure S19a and S19b, when $NaBH_4$ is added, the peak position is basically unchanged. As shown in Figure S19c and S19d, the conversion time of $C_6H_4ClNO_2$ and NB is about 180 s and 450 s, respectively. It indicates that the catalyst also shows good activity for other nitroaromatic hydrocarbons.